Hindawi
Mathematical Problems in Engineering
Volume 2020, Article ID 5634194, 17 pages
https://doi.org/10.1155/2020/5634194

Research Article

Natural Frequencies and Mode Shapes of Drill Pipe in Subsea Xmas Tree Installation

Wensheng Xiao,[1] **Haozhi Qin**,[1] **Jian Liu**,[1] **Qi Liu**,[1] **Junguo Cui**,[1] **and Fengde Wang**[2]

[1]*College of Mechanical and Electronic Engineering, China University of Petroleum (East China), Qingdao, Shandong 266580, China*
[2]*College of Mechanical and Electronic Engineering, Shandong University of Science and Technology, Qingdao 266590, China*

Correspondence should be addressed to Haozhi Qin; qinhao_zhi@163.com

Received 7 January 2020; Revised 18 March 2020; Accepted 17 April 2020; Published 14 May 2020

Academic Editor: Jian Li

In this study, experimental and numerical investigations on the vibration characteristics of a drill pipe during the lowering of a subsea Xmas tree were presented. A fourth-order partial differential equation with variable coefficients was established based on Euler–Bernoulli beam theory. The natural frequencies and mode shapes are obtained by using the differential transformation method. Four drill pipe models of different sizes were used in the experiments which were measured using piezoelectric acceleration sensors and fiber Bragg grating sensors, respectively. The factors that affect the natural frequencies and mode shapes, such as length, diameter, lumped mass, and boundary conditions, were analyzed. The results show that all factors have remarkable effects on the natural frequency, but changes in the length and diameter of the pipe have little effect on the mode shapes; the main factors affecting the mode shape are the boundary conditions and lumped mass. The results of the numerical calculation were validated by a comparison with the experimental results and showed good agreement.

1. Introduction

A subsea Xmas tree (hereafter referred to simply as a tree) is a key piece of equipment in a subsea production system and is widely used in deep water [1]. The installation cost and installation risk in deep water have risen rapidly relative to those in shallow water due to the complex combination of waves and currents [2]. A deep water drill pipe (hereafter referred to simply as a pipe), which is a slender and elastic cylinder, may experience vortex-induced vibration (VIV) exerted by currents and waves. Such vibrations due to vortex shedding lead to cyclic stresses and could result in fatigue damage [3]. In order to improve the service life of the drill pipe, the natural frequency of the system is usually separated from the excitation frequency. Therefore, it is necessary to predict the natural frequency and mode shape of the pipe.

The power series method, the Wentzel–Kramers–Brillouin (WKB) method, the dynamic stiffness method, the variable conversion technique, and other numerical methods have been applied to calculate the vibration characteristics of cylindrical structures such as the pipe or marine risers. Dareing and Huang [3] used the power series method to solve the vibration partial differential equation and obtained an approximate solution for the frequencies of the riser operating in water depths up to 600 ft. Soltanahmadi [4] presented a method based on Fourier analysis to determine the natural frequencies of systems containing either single and multiple flexible risers from the numerically predicted results; this method showed good results in comparison with the linearization method studied by Triantafyllou and Bliek [5]. A simplified analytical approach was proposed by Sparks [6] to examine the physics of the transverse modal vibrations of risers induced by VIV; he believed the flexural rigidity (EI) generally has a small influence on the natural frequency of deep water riser in the low-frequency domain. Considering internal flows, Krawczyk [7] used the Galerkin finite element method to find the fundamental natural frequencies for various internal

flows by neglecting the flexural stiffness of the riser; it was also found that the fundamental natural frequency decreases as the velocity of the internal fluid increases. Montoya-Hernández et al. [8] presented a numerical algorithm to evaluate the natural frequency of marine production risers under internal multiphase flow, in which the riser behavior is affected by the internal fluid density. The solution of the nonlinear partial differential equation involves variable coefficients that cause research on the dynamic responses of marine risers to be highly complex [9], as it is evident in equation (1) later in this paper. In previous research, authors usually simplified the governing equation by ignoring the flexural rigidity and assuming a uniform tension. Although this method is considered to be effective, the accuracy of this approach was found to be limited to low-mode frequencies.

In addition to practical marine engineering researchers, theoretical researchers have focused on the vibration analysis of tensioned beams. Howson and Williams [10] presented a convenient dynamic stiffness matrix method to analyze the natural frequencies of Timoshenko beam under constant tension. The WKB-based dynamic stiffness method [11] has been applied to study the nonuniform marine risers based on the assumption that the properties within risers slowly vary. Based on the Wittrick–Williams algorithm, Si et al. [12] presented a new Newton-type method for nonlinear eigenvalue problems that results in secure second-order convergence at natural frequencies and on mode vectors. Xi et al. [13] investigated the free transverse vibrations of standing and hanging Rayleigh beam-columns subjected to a vertically orientated gravity load; by seeking a nontrivial solution of the partial differential equation of motion for the transverse deflection, the natural frequencies and mode shapes of the beam-columns were calculated. In addition, through both experimental and theoretical analyses, Virgin et al. [14] confirmed that the natural frequencies of very slender vertical cantilevers are affected by their orientation due to gravity. In addition, Anye and Ziguo [15] transformed the fourth order differential equation of a Rayleigh beam into a second-order Fredholm integral equation and obtained the frequency equation by the integral equation method.

The differential transformation method (DTM) is particularly effective when solving the initial and boundary value problem of the nonlinear partial differential equations [16], and thus has been used with some success in applied mathematics in recent years. The DTM, a transformation technique based on Taylor series expansion, is used to solve the ordinary and partial differential equation approximately [17]. This method reduces the governing differential equation and the boundary conditions to a set of algebraic equations according to certain transformation rules. Hence, the DTM is treated as an iterative procedure to get higher order series. Mei [18] applied DTM to analyze the free lateral vibrations of a centrifugally stiffened rotating Euler–Bernoulli beam and obtained the natural frequencies and mode shapes. Ho and Chen [19] solved the free and forced vibration problems of a general elastically end-restrained nonuniform beam resting on a nonhomogeneous elastic foundation and subjected to axial tensile and transverse forces. Chen et al. [9] used the DTM to calculate the natural frequency of a marine riser and compared their findings with the numerical and experimental results obtained by other methods.

Regarding the vibrations of circular slender rod-like structures such as marine risers or drill pipes, most previous studies used boundary conditions in which the ends are fixed or hinged. In recent years, scholars have performed many studies on the vibration characteristics of cylindrical structures such as drill risers or drill pipes; however, most of these investigations focused on risers in working environments, whereas the vibration characteristics of risers or pipes during the installation process have not been frequently reported.

In this paper, the DTM is applied to solve the vibration problems of a suspended pipe. The governing differential equation is transformed into a recursive algebraic equation, and the boundary conditions are also transformed into simple algebraic equations. Thus, the difficulty of solving governing differential equation is greatly reduced. Furthermore, the analytical model is validated by comparing the experimentally measured natural frequencies of a marine riser model with the predicted ones.

2. Mathematical Model

2.1. Governing Equation. In the process of installing a tree, the top of the pipe is connected with a vessel through rigid coupling [20], and the bottom is connected to the tree as a lumped mass. The pipe is subjected to the axial tension force generated by the self-weight and the tree weight and also the lateral force generated by the combined action of wave and current, as shown in Figure 1(a).

To conveniently calculate and derive the formula, the following assumptions are applied during the deduction of the governing equation:

(i) The material of the drill pipe is linearly elastic, isotropous, and homogeneous.

(ii) The outer pipe diameter is constant.

(iii) The mechanical characteristics of the pipe are measured under large deformation with a small strain:

$$\frac{\partial^2}{\partial z^2}\left(E(x)I(x)\frac{\partial^2 x(z,t)}{\partial z^2}\right) - \frac{\partial}{\partial z}\left(T(z)\frac{\partial x(z,t)}{\partial z}\right) + m_e(z)\frac{\partial^2 x(z,t)}{\partial t^2} = 0. \tag{1}$$

In equation (1), t is the time; z is the coordinate measured along the axis of the pipe; $x(z, t)$ is the transverse deflection of the beam axis and is a function of the vertical coordinate z and time t; $E(x)$ is the modulus of elasticity; $I(x)$ is the area moment of inertia; $m_e(z)$ is the effective mass of the pipe per unit length; and $T(z)$ is the axial tension force of the beam.

For a hang-off drilling pipe, $T(z)$ can be represented by the following:

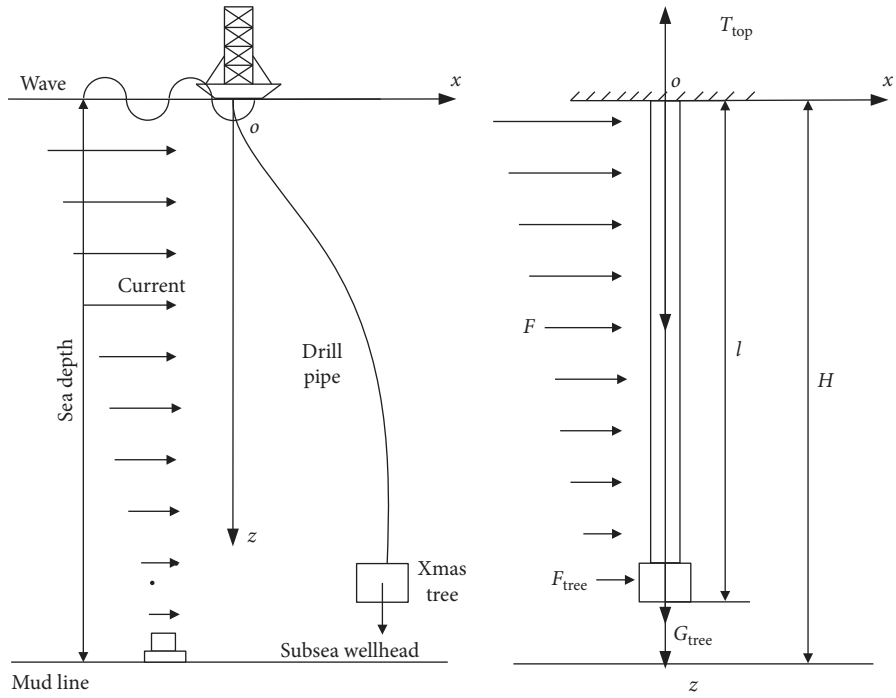

Figure 1: (a) Schematic diagram and (b) mechanical analysis model for the subsea Xmas tree installation process.

$$\left.\begin{aligned} w &= \frac{1}{4}\pi g\left(\rho_s - \rho_w\right)\left(D^2 - d^2\right), \\ T(z) &= m_B g + \int_z^l w\,dz, \end{aligned}\right\} \tag{2}$$

where z is the distance from the section to the top of the pipe; $w(z)$ is the net weight of the pipe (per unit length); $m_B g$ is the suspend weight at the pipe bottom, i.e., the combined weight of the tree and installation tool; ρ_s is the density of the pipe; ρ_w is the density of seawater; and D and d are the outer and inner diameters of the pipe, respectively.

The effective mass of the pipe per unit length includes the pipe body, internal fluid, and added mass. $m_e(z)$ is calculated by

$$\left.\begin{aligned} m_e(z) &= m_p + m_f + m_a, \\ m_p &= \frac{1}{4}\pi\rho_s\left(D^2 - d^2\right), \\ m_f &= \frac{1}{4}\pi\rho_f d^2, \\ m_a &= \frac{1}{4}\pi C_a \rho_w D^2, \end{aligned}\right\} \tag{3}$$

where m_p is the mass of the pipe; m_f is the mass of the internal fluid; m_a is the added mass; C_a is the added mass factor; and ρ_f is the density of the internal fluid. The internal and external fluids are both seawater with the same density because seawater can flow freely into the pipe from the bottom of the tree during the lowering process.

Equation (4) presents the boundary conditions of the pipe at $z = 0$ and $z = l$:

$$\left.\begin{aligned} &x(z,t)\big|_{z=0} = 0, \\ &\left.\frac{\partial x(z,t)}{\partial z}\right|_{z=0} = 0, \\ &-E(z)I(x)\left.\frac{\partial^3 x(z,t)}{\partial z^3}\right|_{z=l} + T(z)\frac{\partial x(z,t)}{\partial z} = -m_B(z)\left.\frac{\partial^2 x(z,t)}{\partial t^2}\right|_{z=l}, \\ &\left.E(z)I(x)\frac{\partial^2 x(z,t)}{\partial z^2}\right|_{z=l} = 0. \end{aligned}\right\} \tag{4}$$

In order to solve equation (1), the separation of variable method is used as follows:

$$x(z,t) = \varphi(z)\gamma(t), \tag{5}$$

where the lateral deflection of the pipe is expressed as the product of a spatial function $\varphi(z)$ and a temporal function $\gamma(t)$.

The governing equation of the pipe can be deduced by substituting equation (5) into equation (1) as follows:

$$\begin{aligned} &\frac{\partial^2}{\partial z^2}\left(E(z)I(z)\frac{\partial^2\varphi(z)}{\partial z^2}\right) - \frac{\partial}{\partial z}\left(T(z)\frac{\partial\varphi(z)}{\partial z}\right) \\ &\quad - m_e(z)\omega^2\varphi(z) = 0. \end{aligned} \tag{6}$$

The boundary condition equations of the pipe can be converted into a new form by substituting equation (5) into equation (4) as follows:

$$\left.\begin{aligned}
&\varphi(z)\,|_{z=0} = 0,\\
&\left.\frac{\partial\varphi(z)}{\partial z}\right|_{z=0} = 0,\\
&-E(z)I(z)\left.\frac{\partial^3\varphi(z)}{\partial z^3}\right|_{z=l} + T(z)\frac{\partial\varphi(z)}{\partial z} = -m_{\mathrm{B}}(z)\omega^2\varphi(z)\,|_{z=l},\\
&\left.E(z)I(z)\frac{\partial^2\varphi(z)}{\partial z^2}\right|_{z=l} = 0.
\end{aligned}\right\} \tag{7}$$

2.2. Dimensionless Transformation. Two nondimensional parameters:

$$\begin{aligned}
\overline{z} &= \frac{z}{l},\\
\overline{\varphi} &= \frac{\varphi}{l}.
\end{aligned} \tag{8}$$

Using a spectral representation [21], equation (6) can be written as follows:

$$\begin{aligned}
&\frac{\partial^2}{\partial\overline{z}^2}\left(E(z)I(z)\frac{\partial^2\varphi(\overline{z})}{\partial\overline{z}^2}\right) - l^2\frac{\partial}{\partial\overline{z}}\left(T(z)\frac{\partial\varphi(\overline{z})}{\partial\overline{z}}\right)\\
&\quad - m_{\mathrm{e}}(\overline{z})\omega^2 l^4\varphi(\overline{z}) = 0.
\end{aligned} \tag{9}$$

Both sides of equation (6) are then divided by $E(0)\,I(0)$:

$$\begin{aligned}
&\frac{\partial^2}{\partial\overline{z}^2}\left(\frac{E(z)I(z)}{E(0)I(0)}\frac{\partial^2\varphi(\overline{z})}{\partial\overline{z}^2}\right) - \frac{\partial}{\partial\overline{z}}\left(\frac{l^2T(z)}{E(0)I(0)}\frac{\partial\varphi(\overline{z})}{\partial\overline{z}}\right)\\
&\quad - \frac{m_{\mathrm{e}}(\overline{z})\omega^2 l^4}{E(0)I(0)}\varphi(\overline{z}) = 0,
\end{aligned} \tag{10}$$

where the following dimensionless quantities can be defined:

$$\begin{aligned}
a(\overline{z}) &= \frac{E(z)I(z)}{E(0)I(0)},\\
b(\overline{z}) &= \frac{l^2T(z)}{E(0)I(0)},\\
q(\overline{z}) &= \frac{m_{\mathrm{e}}(\overline{z})}{m_{\mathrm{e}}(0)},\\
\lambda^4 &= \frac{m_{\mathrm{e}}(0)\omega^2 l^4}{E(0)I(0)}.
\end{aligned} \tag{11}$$

Equation (10) can be written as follows:

$$\frac{\partial^2}{\partial\overline{z}^2}\left(a(\overline{z})\frac{\partial^2\varphi(\overline{z})}{\partial\overline{z}^2}\right) - \frac{\partial}{\partial\overline{z}}\left(b(\overline{z})\frac{\partial\varphi(\overline{z})}{\partial\overline{z}}\right) - q(\overline{z})\lambda^4\varphi(\overline{z}) = 0. \tag{12}$$

The same dimensionless treatment method is used, and the nondimensional boundary conditions become

$$\left.\begin{aligned}
&\varphi(\overline{z})\,|_{\overline{z}=0} = 0,\\
&\left.\frac{\partial\varphi(\overline{z})}{\partial\overline{z}}\right|_{\overline{z}=0} = 0,\\
&a(\overline{z})\left.\frac{\partial^3\varphi(\overline{z})}{\partial\overline{z}^3}\right|_{\overline{z}=l} - b(\overline{z})\frac{\partial\varphi(\overline{z})}{\partial\overline{z}} - \zeta_{\mathrm{m}}\lambda^2\varphi(\overline{z})\,|_{\overline{z}=l} = 0,\\
&\left.\frac{\partial^2\varphi(\overline{z})}{\partial\overline{z}^2}\right|_{\overline{z}=l} = 0,
\end{aligned}\right\} \tag{13}$$

where $\zeta_{\mathrm{m}} = m_{\mathrm{B}}/m_{\mathrm{e}}(0)l$.

2.3. Extracting the Frequencies and Mode Shapes by the DTM. The differential transformation of the kth-order derivative of a function $\phi(z)$ is represented as follows:

$$\Phi(k) = \frac{1}{k!}\left[\frac{\partial^k\varphi(\overline{z})}{\partial\overline{z}^k}\right]\Bigg|\overline{z} = \overline{z}_0, \quad 0 \le \overline{z} \le 1, \tag{14}$$

where $\Phi(k)$ is referred to as the kth-order differential transformation (T-function) at the point $x = x_0$. $x_0 = 0$ is usually assumed for convenience but is not necessary. The inverse differential transformation can be written in the following form:

$$\varphi(\overline{z}) = \sum_k^{\infty}(\overline{z} - \overline{z}_0)^k\frac{1}{k!}\left[\frac{\partial^k\varphi(\overline{z})}{\partial\overline{z}^k}\right] = \sum_k^{\infty}(\overline{z} - \overline{z}_0)^k\Phi(k). \tag{15}$$

Equation (15) implies that the DTM is derived from Taylor series expansion of the function $\phi(z)$ at $z = z_0$.

The fundamental transformation rules [22] are listed in Table 1.

Based on the differential transformation of equation (14) and the basic operations in Table 1, the governing equation in equation (12) can be converted into the following recursive equation:

$$\begin{aligned}
&\sum_{r=0}^{k}A(k-r)(r+1)(r+2)(r+3)(r+4)\Phi(r+4)\\
&\quad + 2\sum_{r=0}^{k}(k-r+1)A(k-r+1)(r+1)(r+2)(r+3)\Phi(r+3)\\
&\quad + \sum_{r=0}^{k}(k-r+1)(k-r+2)A(k-r+2)(r+1)(r+2)\Phi(r+2)\\
&\quad - \sum_{r=0}^{k}B(k-r)(r+1)(r+2)\Phi(r+2)\\
&\quad - \sum_{r=0}^{k}(k-r+1)B(k-r+1)(r+1)\Phi(r+1)\\
&\quad = \lambda^4\Phi(r)Q(k-r),
\end{aligned} \tag{16}$$

Table 1: Basic operations for applications of differential transformation.

Original function $f(z)$	Transformed function $F(k)$
$f(z) = \lambda g(z)$	$F(k) = \lambda G(k)$
$f(z) = g(z) \pm h(z)$	$F(k) = G(x) \pm H(k)$
$f(z) = g(z)h(z)$	$F(k) = \sum_{r=0}^{k} G(r) \pm H(k-r)$
$f(z) = g_1(z)g_2(z)\cdots g_{n-1}(z)g_n(z)$	$F(k) = \sum_{k_{n-1}=0}^{k} \sum_{k_{n-2}=0}^{k_{n-1}} \cdots \sum_{k_2=0}^{k_3} \sum_{k_1=0}^{k_2} G_1(k_1)G_2(k_2-k_1)\cdots G_{n-1}(k_{n-1}-k_{n-2})G_n(k_n-k_{n-1})$
$f(z) = (\mathrm{d}^k g(z))/\mathrm{d}x^k$	$F(k) = (k+1)(k+2)\cdots(k+i)G(k+i)$

where $\Phi(k)$, $A(k)$, $B(k)$, and $Q(k)$ are the transformed functions of $\phi(z)$, $a(z)$, $b(z)$, and $q(z)$, respectively.

The transformed boundary condition equations can be deduced by substituting equation (15) into equation (13) as follows:

$$\left.\begin{aligned}
&\sum_{k=0}^{\infty} (\overline{z}-\overline{z}_0)^k \Phi(k)\Big|_{\overline{z}=0} = 0,\\
&\sum_{k=0}^{\infty} k(\overline{z}-\overline{z}_0)^{(k-1)} \Phi(k)\Big|_{\overline{z}=0} = 0,\\
&a(\overline{z}) \sum_{k=0}^{\infty} k(k-1)(k-2)(\overline{z}-\overline{z}_0)^{(k-3)} \Phi(k)\Big|_{\overline{z}=1} - b(\overline{z}) \sum_{k=0}^{\infty} k(\overline{z}-\overline{z}_0)^{(k-1)} \Phi(k)\Big|_{\overline{z}=1} + \zeta_{\mathrm{m}}\lambda^2 \sum_{k=0}^{\infty} (\overline{z}-\overline{z}_0)^k \Phi(k)\Big|_{\overline{z}=1} = 0,\\
&\sum_{k=0}^{\infty} k(k-1)(\overline{z}-\overline{z}_0)^{(k-2)} \Phi(k)\Big|_{\overline{z}=1} = 0.
\end{aligned}\right\} \tag{17}$$

Considering that equation (16) is a recursive formula; suppose $\Phi(0) = \xi 1$, $\Phi(1) = \xi 2$, $\Phi(2) = \xi 3$, and $\Phi(3) = \xi 4$; therefore, $\Phi(\mathrm{k})$ can be represented by $\xi 1$, $\xi 2$, $\xi 3$, and $\xi 4$. Then, substitute these terms into the four boundary conditions of equation (17). A set of homogeneous equations of quaternion polynomials can be obtained, which can be assembled into a matrix equation of the following form:

$$[A]_{4\times 4}\{\xi_1, \xi_2, \xi_3, \xi_4\}_{1\times 4}^{\mathrm{T}} = 0, \tag{18}$$

where $[A]$ is the coefficient matrix of equation (15). In order to ensure that equation (18) has nontrivial solutions, the determinant of matrix $[A]$ must be equal to zero, which will reveal an nth-order polynomial about the eigenvalue λ. Thus, the eigenvalue λ can be obtained by solving the polynomial and subsequently solving for the natural frequency of the pipe as follows:

$$\omega = \frac{\lambda^2}{l^2}\sqrt{\frac{EI}{m_{\mathrm{e}}}}. \tag{19}$$

The mode shapes of the pipe can be obtained once the values of λ are found. By setting $\xi 1 = 1$, $\xi 2$, $\xi 3$, and $\xi 4$ can be determined by substituting λ into equation (18). After obtaining $\xi 1 \sim \xi 4$, the $\Phi(k)$ can be generated by equation (16), which will allow the mode shape to be solved by the differential inverse transformation of equation (15), which can be subsequently normalized as follows [22]:

$$\varphi(z) = \frac{\varphi(z)}{\int_0^1 |\varphi(z)|\mathrm{d}z}. \tag{20}$$

3. Model Experiment

3.1. Experiment Set. In order to verify whether the method can be used to calculate the frequency of the pipe when lowering a subsea Xmas tree, four drill pipe models of different sizes were made from stainless steel (SUS 304), and their properties are listed in Table 2. The top end of the model was fixed on the bracket and the bottom part was set to be free as a lumped mass, as shown in Figure 2. The experiment was carried out in a tank (1500 mm long × 800 mm wide × 950 mm deep) which was designed and constructed for water research. Water flowed freely in the model, and we assumed that the entrained water in the simulation scheme vibrate with the model.

Two kinds of sensors were used to test the natural frequency of model: the piezoelectric acceleration (PA) sensor and the fiber Bragg grating (FBG) sensor. As shown in Figure 2, the optical sensing interrogator, which has a full spectrum at 5 kHz with 80 nm and a wavelength accuracy of 2 pm/3 pm, was used to detect optical signals from the FBG sensor. The PA sensor signal was collected and processed by a DH5902N data acquisition and analysis system with a 2 kHz sampling rate.

Seven locations were selected to place the PA sensors and FBG sensors; their arrangements are shown in Figure 3. "x_1" was used to capture the x-axis vibration, and "y_2" was used to capture the y-axis vibration.

3.2. Test Content. In this paper, we carried out oscillating experiments in still water. The values of the diameter D and

Table 2: Characteristics of the pipe model.

Property	Value			
	Model 1	Model 2	Model 3	Model 4
Length of the pipe (l) m	0.9	1.5	0.9	1.5
Outside diameter (D) mm	10	10	40	40
Thickness of pipe (δ) mm	1	1	2.3	2.3
Density of drill pipe (ρs) kg/m^3	7930	7930	7930	7930
Elastic modulus of steel (E) GPa	206	206	206	206
Add mass coefficient (C_a)	1	1	1	1
Bottom mass of model (W_B) kg	0~0.55	0~0.55	0~5	0~5

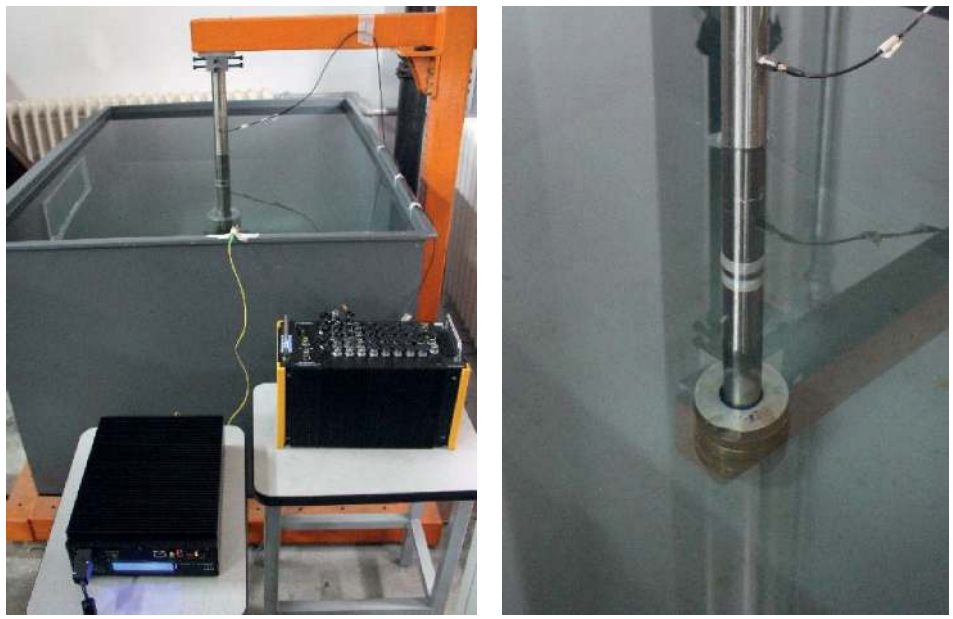

(a) (b)

Figure 2: Riser pipe model and its part. (a) Pipe model and measuring devices and (b) part of the pipe model.

the lumped mass m used in experiment for all test cases are listed in Table 3.

3.3. DTM. Since the pipe model adopted in this paper is uniform in the whole length direction, the governing equation of equation (10) can be simplified as follows:

$$\frac{d^4\varphi(\overline{z})}{d\overline{z}^4} - \frac{d}{d\overline{z}}\left((\alpha - \beta\overline{z})\frac{d\varphi(\overline{z})}{d\overline{z}}\right) - \lambda^4\varphi(\overline{z}) = 0, \quad (21)$$

where $\alpha = (l^2/EI)(wl + m_B g)$, $\beta = wl^3/EI$, and $\lambda^4 = m_e\omega^2 l^4/EI$. Equation (16) can be correspondingly converted into the following recursive equation using the DTM:

$$\Phi(k+4) = \frac{(\mu + \nu x_0)\Phi(k+2)}{(k+3)(k+4)} + \frac{\nu(k+1)\Phi(k+1)}{(k+2)(k+3)(k+4)} + \frac{\lambda^4\Phi(k)}{(k+1)(k+2)(k+3)(k+4)}. \quad (22)$$

3.4. Experimental Results. Table 4 shows the error in the prediction of the natural frequencies of the model pipe, where the error is defined as the percentage of the ratio of the absolute difference between experimental values and theoretical calculating values. Error1 is the error between value measured by the PA sensor and the theoretical calculating value; the maximum error occurs at the fourth frequency of Exp20, and the error is 15.53%, while the minimum error is 0.04%, which occurs at the fourth frequency of Exp10, and the average error is less than 5%. Error2 represents the error between the value from the FBG sensor and the theoretical calculating value; the maximum error is 8.93%, which occurs at the fifth frequency of Exp22, while the smallest error is 0.05% for the fifth frequency of Exp21, and the mean error is 2.8%. Error3 is the error between the two experimental sensors, and the mean error is 3.09%. The frequency obtained using the DTM is acceptable enough for design purposes because the mean error is generally less than 5%; thus, the frequency of the pipe when lowering a subsea Xmas tree can be determined using the equations and technique proposed in this paper.

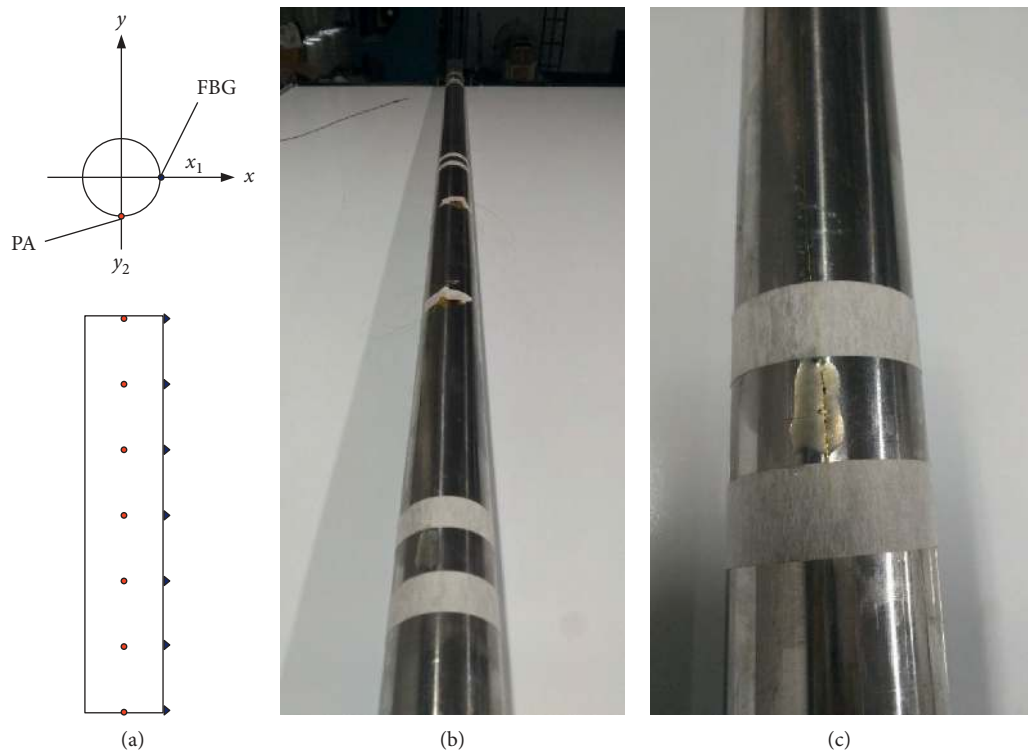

Figure 3: Schematic view of the pipe model and measuring points in experiment: (a) a schematic diagram of sensors, (b) a picture of pipe model with sensors, and (c) sensors.

Table 3: Experimental conditions.

	The diameter D (mm)	Pipe length L (mm)	The lumped mass: m (g)					
			0	103	206	309	412	515
Model 1	10	900	Exp1	Exp2	Exp3	Exp4	Exp5	Exp6
Model 2	10	1500	Exp7	Exp8	Exp9	Exp10	Exp11	Exp12
	The diameter D (mm)	Pipe length L (mm)	The lumped mass: m (g)					
			0	1155	2097	3032	3972	4912
Model 3	40	900	Exp13	Exp14	Exp15	Exp16	Exp17	Exp18
Model 4	40	1500	Exp19	Exp20	Exp21	Exp22	Exp23	Exp24

Figure 4 shows a plot of the experimentally measured natural frequencies of the model pipe in still water in comparison with the natural frequencies predicted by the DTM using the equations developed in this paper. Results of experimental tests prove that the theoretical calculating values match well with the experimental measuring values.

By comparing the curve of Exp1 with that of Exp7 or by comparing the curve of Exp13 with that of Exp19 in Figure 5, it can be observed that as the length of the pipe model increases, the natural frequencies of each order decreases, and thus, it can be inferred that the natural frequency of the system decreases gradually during the process of lowering the pipe. At the same time, by comparing the curve of Exp1 with that of Exp13 or by comparing the curve of Exp7 with that of Exp19, it can be seen that the specification of the pipe is an important factor affecting the natural frequency of the system. In the case of the same length, the larger the diameter of the pipe is, the higher the natural frequency of each order will be.

The effect of the lumped mass at the bottom of the pipe on the natural frequency of the model pipe 1 is plotted in Figure 6. It is obvious from Figure 6 that the natural frequency of the pipe model decreases with increasing bottom weight, and the results obtained by the two experimental sensors are consistent with the theoretical calculation. Therefore, in an actual project, the weight of the Xmas tree has a significant impact on the frequency of the whole lowering system.

Figure 7(a)–7(f) show the mode shapes of the pipe model; these modes are obtained by the DTM and FBG sensor, respectively. It can be seen that the first five mode shapes obtained by the theoretical method and experimental sensor are basically coincident. The mode shapes of the pipe can be determined using the equations and technique proposed in this paper. However, the amplitudes of the

Table 4: Error of predicted natural frequencies in experimental cases.

Case	Natural frequency	Theoretical value	PA	FBG	Error1 (%)	Error2 (%)	Error3 (%)
Exp1	1st	10.5147	10.7863	10.3401	2.58	1.66	4.14
	2nd	65.8235	60.4248	63.2812	8.20	3.86	4.73
	3rd	184.2873	174.5605	176.1025	5.28	4.44	0.88
	4th	361.1188	345.4591	345.3308	4.34	4.37	0.04
	5th	596.9475	562.7441	580.5326	5.73	2.75	3.16
	6th	891.7300	825.1953	825.3219	7.46	7.45	0.02
Exp2	1st	6.5076	7.3243	6.2983	12.55	3.22	14.01
	2nd	51.3432	48.8281	50.5211	4.90	1.60	3.47
	3rd	155.5492	151.3672	153.6025	2.69	1.25	1.48
	4th	318.0149	313.1104	312.9178	1.54	1.60	0.06
	5th	539.2983	520.6299	520.6002	3.46	3.47	0.01
	6th	819.4665	800.2637	810.2438	2.34	1.13	1.25
Exp3	1st	5.1823	5.4145	5.0371	4.48	2.80	6.97
	2nd	49.1996	47.6074	47.5933	3.24	3.26	0.03
	3rd	152.8061	150.7568	152.4119	1.34	0.26	1.10
	4th	315.0362	310.3311	311.5492	1.49	1.11	0.39
	5th	536.1817	515.8887	517.5979	3.78	3.47	0.33
	6th	816.2613	788.8086	797.3321	3.36	2.32	1.08
Exp4	1st	4.4392	4.8828	4.1414	9.99	6.71	15.18
	2nd	48.3092	47.6074	47.6291	1.45	1.41	0.05
	3rd	151.7448	149.5361	150.2124	1.46	1.01	0.45
	4th	313.9227	307.0068	310.4764	2.20	1.10	1.13
	5th	535.0382	509.0332	516.1435	4.86	3.53	1.40
	6th	815.0991	787.5117	793.8137	3.38	2.61	0.80
Exp5	1st	3.9487	3.8521	3.8828	2.45	1.67	0.80
	2nd	47.8260	47.6074	47.4852	0.46	0.71	0.26
	3rd	151.1870	147.0947	148.7914	2.71	1.58	1.15
	4th	313.3460	296.6309	307.1457	5.33	1.98	3.54
	5th	534.4506	490.957	515.0786	8.14	3.62	4.91
	6th	814.5047	781.6836	789.8112	4.03	3.03	1.04
Exp6	1st	3.5945	3.6828	3.4392	2.46	4.32	6.61
	2nd	47.5255	46.9971	46.9573	1.11	1.20	0.08
	3rd	150.8466	144.8877	140.8317	3.95	6.64	2.80
	4th	312.9971	294.8539	297.3333	5.80	5.00	0.84
	5th	534.0966	487.3223	513.5267	8.76	3.85	5.38
	6th	814.1477	779.2041	782.8726	4.29	3.84	0.47
Exp7	1st	3.6311	3.9196	3.7399	7.94	3.00	4.58
	2nd	22.6353	24.4731	22.8863	8.12	1.11	6.48
	3rd	63.3445	66.7916	61.7196	5.44	2.57	7.59
	4th	124.1114	118.3987	120.8129	4.60	2.66	2.04
	5th	205.1518	192.9841	197.6397	5.93	3.66	2.41
	6th	306.4508	281.2845	300.1003	8.21	2.07	6.69
Exp8	1st	2.6204	2.8489	2.7537	8.72	5.09	3.34
	2nd	18.4668	19.3654	18.2873	4.87	0.97	5.57
	3rd	54.6145	60.4631	57.3336	10.71	4.98	5.18
	4th	110.6133	116.6287	112.7168	5.44	1.90	3.35
	5th	186.7600	192.7039	189.0539	3.18	1.23	1.89
	6th	283.1069	270.4674	274.4444	4.46	3.06	1.47
Exp9	1st	2.1833	2.3416	2.2396	7.25	2.58	4.36
	2nd	17.5189	18.8431	18.0539	7.56	3.05	4.19
	3rd	53.2767	57.9743	55.8113	8.82	4.76	3.73
	4th	109.0850	112.8	110.3336	3.41	1.14	2.19
	5th	185.1139	189.7431	185.6987	2.50	0.32	2.13
	6th	281.3824	269.1264	273.1249	4.36	2.93	1.49

Table 4: Continued.

Case	Natural frequency	Theoretical value	PA	FBG	Error1 (%)	Error2 (%)	Error3 (%)
Exp10	1st	1.9161	2.1341	2.0223	11.38	5.54	5.24
	2nd	17.0886	16.4631	17.2574	3.66	0.99	4.82
	3rd	52.7259	54.7598	53.7434	3.86	1.93	1.86
	4th	108.4875	108.4394	109.2253	0.04	0.68	0.72
	5th	184.4890	183.3648	183.5464	0.61	0.51	0.10
	6th	280.7400	265.153	265.3254	5.55	5.49	0.07
Exp11	1st	1.7319	1.8821	1.7746	8.67	2.46	5.71
	2nd	16.8468	16.1428	16.3394	4.18	3.01	1.22
	3rd	52.4307	51.3689	51.8531	2.03	1.10	0.94
	4th	108.1746	106.2254	107.1038	1.80	0.99	0.83
	5th	184.1660	179.6413	177.6599	2.46	3.53	1.10
	6th	280.4105	261.2791	260.7397	6.82	7.01	0.21
Exp12	1st	1.5955	1.7325	1.7365	8.58	8.83	0.23
	2nd	16.6945	15.9542	15.9987	4.43	4.17	0.28
	3rd	52.2501	49.254	48.4355	5.73	7.30	1.66
	4th	107.9857	103.3634	105.3333	4.28	2.46	1.91
	5th	183.9724	174.9213	176.5189	4.92	4.05	0.91
	6th	280.2139	254.3864	259.2547	9.22	7.48	1.91
Exp13	1st	36.8698	34.4861	6.47%	3.05	3.65	6.47
	2nd	231.0448	223.3359	3.34%	0.50	2.93	3.34
	3rd	646.9281	673.7881	4.15%	0.60	3.41	4.15
	4th	1267.7187	1307.829	3.16%	3.38	0.21	3.16
	5th	2095.6284	2345.238	11.91%	8.86	2.72	11.91
	6th	3130.5047	3380.716	7.99%	5.38	2.42	7.99
Exp14	1st	23.7641	25.9533	22.6144	9.21	4.84	12.87
	2nd	182.1634	192.5408	189.4824	5.70	4.02	1.59
	3rd	548.7162	520.1795	540.8744	5.20	1.43	3.98
	4th	1119.4019	999.7836	1089.3244	10.69	2.69	8.96
	5th	1896.4459	1785.127	1823.8248	5.87	3.83	2.17
	6th	2880.1461	2769.759	2898.0893	3.83	0.62	4.63
Exp15	1st	19.5296	20.2378	18.8513	3.63	3.47	6.85
	2nd	174.6356	187.4995	183.9104	7.37	5.31	1.91
	3rd	538.8244	513.7513	533.0132	4.65	1.08	3.75
	4th	1108.5160	1174.466	1089.7347	5.95	1.69	7.21
	5th	1884.9708	1773.479	1736.2437	5.91	7.89	2.10
	6th	2868.2890	2537.492	2727.3099	11.53	4.92	7.48
Exp16	1st	16.9820	15.713	16.4131	7.47	3.35	4.46
	2nd	171.1710	159.9923	170.0844	6.53	0.63	6.31
	3rd	534.5942	551.7963	547.2145	3.22	2.36	0.83
	4th	1104.0262	1208.198	1137.1944	9.44	3.00	5.88
	5th	1880.3318	1976.187	1901.003	5.10	1.10	3.80
	6th	2863.5560	2761.761	2844.7672	3.55	0.66	3.01
Exp17	1st	15.2184	15.1349	15.2124	0.55	0.04	0.51
	2nd	169.1611	174.3981	177.1978	3.10	4.75	1.61
	3rd	532.2258	530.1284	546.2446	0.39	2.63	3.04
	4th	1101.5536	1194.7641	1116.3345	8.46	1.34	6.56
	5th	1877.7996	1966.9432	1894.1487	4.75	0.87	3.70
	6th	2860.9866	2733.9673	2819.6687	4.44	1.44	3.13
Exp18	1st	13.9106	14.9721	14.1121	7.63	1.45	5.74
	2nd	167.8552	170.9841	172.3347	1.86	2.67	0.79
	3rd	530.7195	526.1192	538.9401	0.87	1.55	2.44
	4th	1099.9959	1181.791	1104.0022	7.44	0.36	6.58
	5th	1876.2124	1951.764	1884.2546	4.03	0.43	3.46
	6th	2859.3811	2710.762	2804.3463	5.20	1.92	3.45

Table 4: Continued.

Case	Natural frequency	Theoretical value	PA	FBG	Error1 (%)	Error2 (%)	Error3 (%)
Exp19	1st	12.6734	13.2563	12.3225	4.60	2.77	7.04
	2nd	79.3990	73.7568	78.4572	7.11	1.19	6.37
	3rd	222.3127	220.3311	224.6267	0.89	1.04	1.95
	4th	435.6404	470.4668	452.6511	7.99	3.90	3.79
	5th	720.1421	802.6058	769.3038	11.45	6.83	4.15
	6th	1075.7656	975.1812	1002.0375	9.35	6.85	2.75
Exp20	1st	9.3936	10.0974	9.8236	7.49	4.58	2.71
	2nd	65.5353	66.8899	66.7954	2.07	1.92	0.14
	3rd	192.8674	207.4506	198.1269	7.56	2.73	4.49
	4th	389.6997	450.232	420.3284	15.53	7.86	6.64
	5th	657.1804	600.2085	650.7065	8.67	0.99	8.41
	6th	995.5286	1063.786	987.8547	6.86	0.77	7.14
Exp21	1st	8.0243	7.7562	7.7034	3.34	4.00	0.68
	2nd	62.2993	58.189	60.8146	6.60	2.38	4.51
	3rd	188.1462	200.0332	192.4503	6.32	2.29	3.79
	4th	384.2031	381.5346	390.6624	0.69	1.68	2.39
	5th	651.1935	644.4566	650.8563	1.03	0.05	0.99
	6th	989.2098	1002.723	990.5333	1.37	0.13	1.22
Exp22	1st	7.1245	6.8512	7.3369	3.84	2.98	7.09
	2nd	60.6575	58.2123	57.8555	4.03	4.62	0.61
	3rd	185.9753	195.3257	189.6279	5.03	1.96	2.92
	4th	381.8073	400.4822	395.1465	4.89	3.49	1.33
	5th	648.6642	710.3375	706.5805	9.51	8.93	0.53
	6th	986.5939	1023.985	992.3503	3.79	0.58	3.09
Exp23	1st	6.4695	6.3356	6.4365	2.07	0.51	1.59
	2nd	59.6564	57.3487	57.0213	3.87	4.42	0.57
	3rd	184.7180	188.2234	185.34623	1.90	0.34	1.53
	4th	380.4551	394.8947	388.1113	3.80	2.01	1.72
	5th	647.2570	690.7536	660.2769	6.72	2.01	4.41
	6th	985.1517	1000.325	980.7383	1.54	0.45	1.96
Exp24	1st	5.9677	6.2872	6.1012	5.35	2.24	2.96
	2nd	58.9858	60.7298	56.3343	2.96	4.50	7.24
	3rd	183.9026	188.9128	180.3843	2.72	1.91	4.51
	4th	379.5914	380.9412	377.5567	0.36	0.54	0.89
	5th	646.3656	660.9734	652.2794	2.26	0.91	1.32
	6th	984.2429	991.5867	980.3444	0.75	0.40	1.13

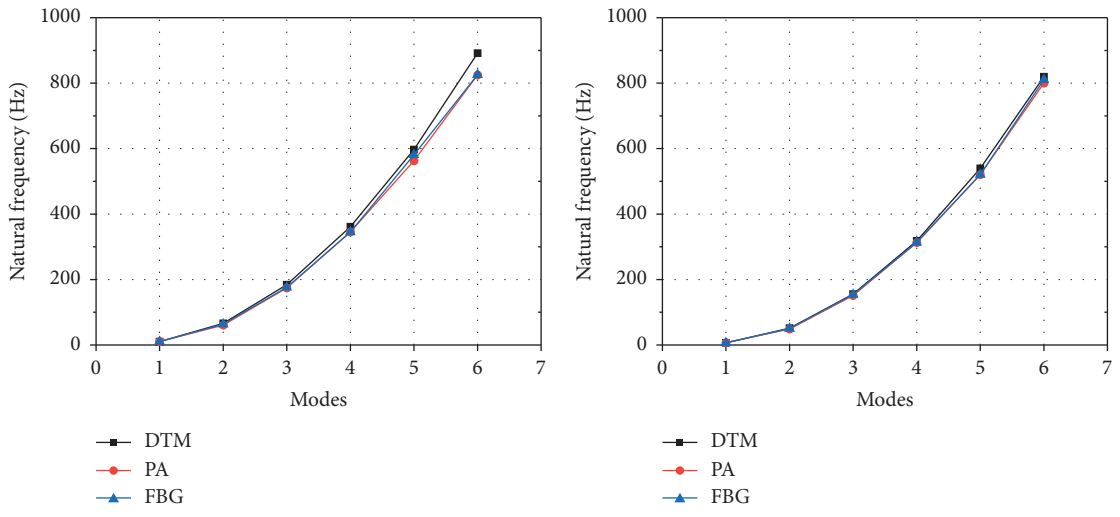

Figure 4: Continued.

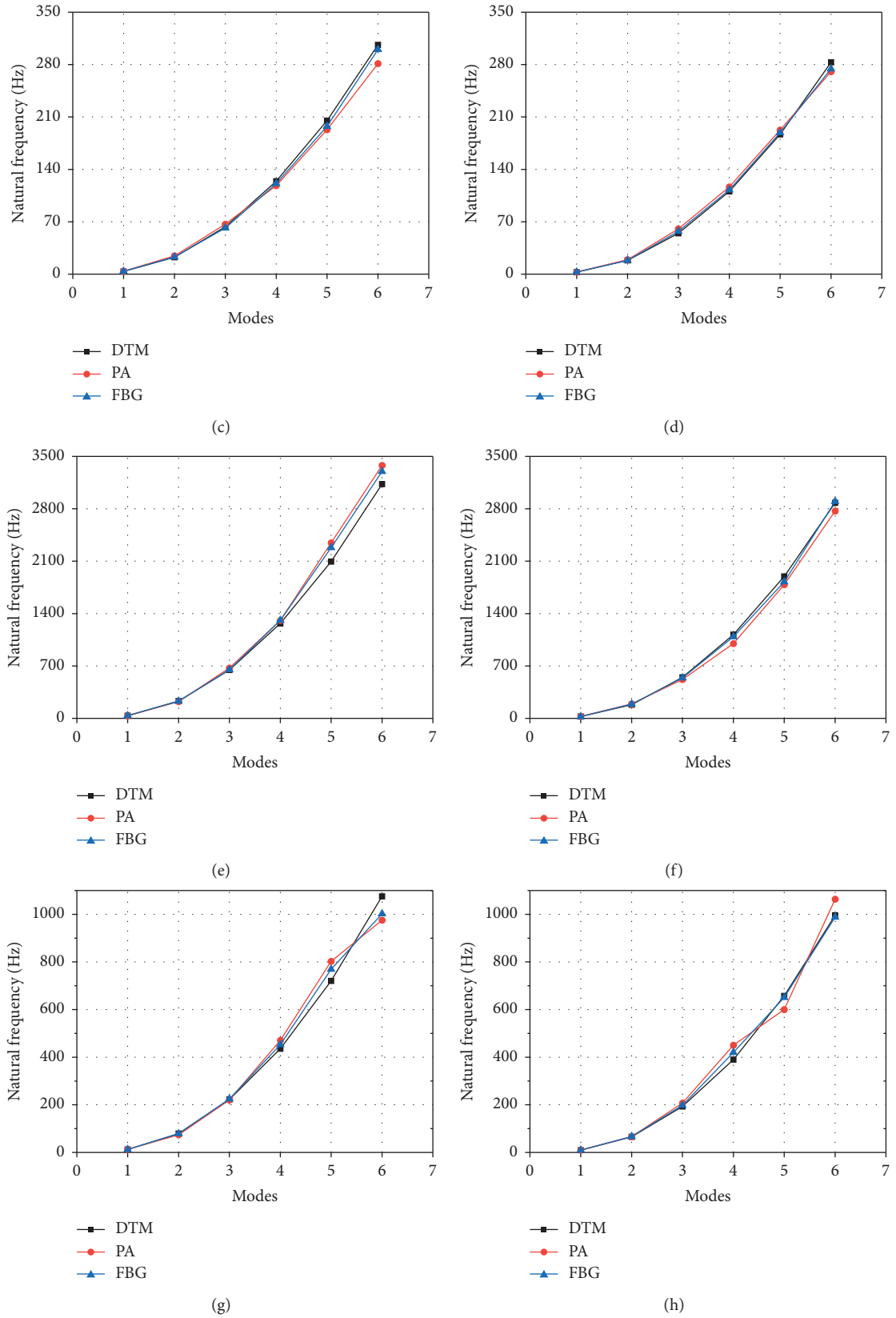

Figure 4: The frequencies of pipes in different methods: (a) model pipe 1 in Exp1, (b) model pipe 1 in Exp2, (c) model pipe 2 in Exp7, (d) model pipe 2 in Exp8, (e) model pipe 3 in Exp13, (f) model pipe 3 in Exp14, (g) model pipe 4 in Exp19, and (h) model pipe 4 in Exp20.

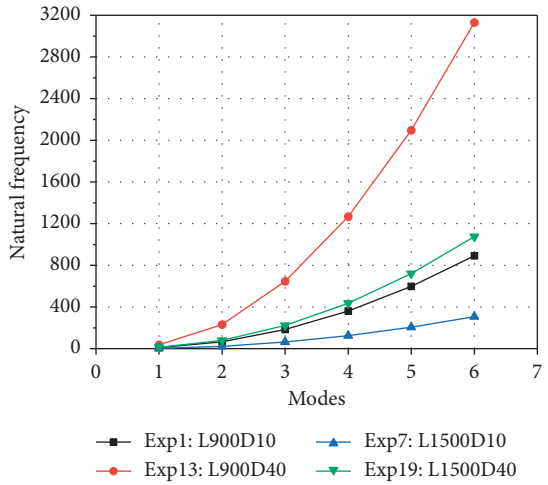

Figure 5: Comparisons of natural frequencies of the model pipe.

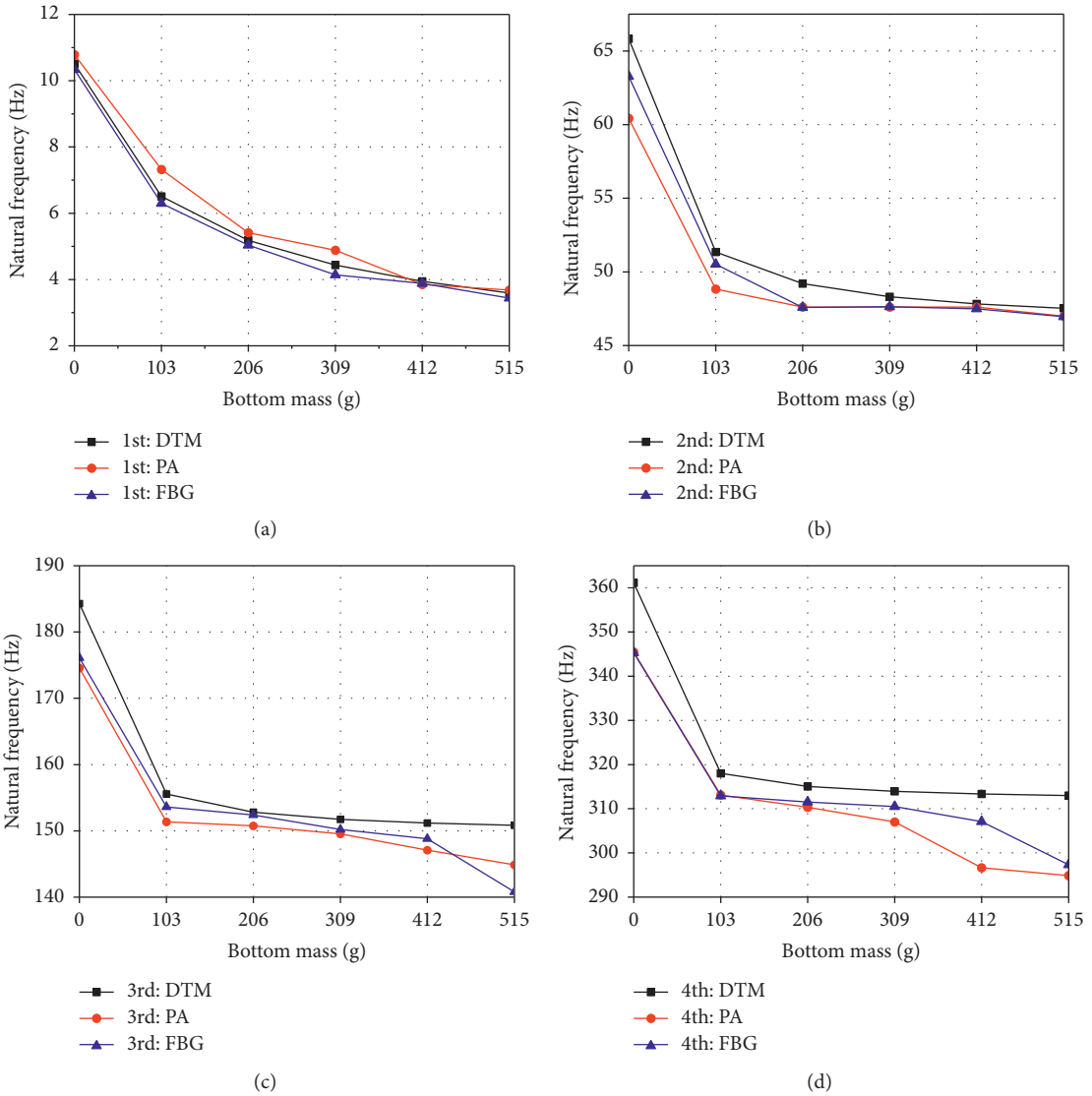

Figure 6: Natural frequencies of the model pipe 1 with a lumped mass: (a) first mode, (b) second mode, (c) third mode, and (d) fourth mode.

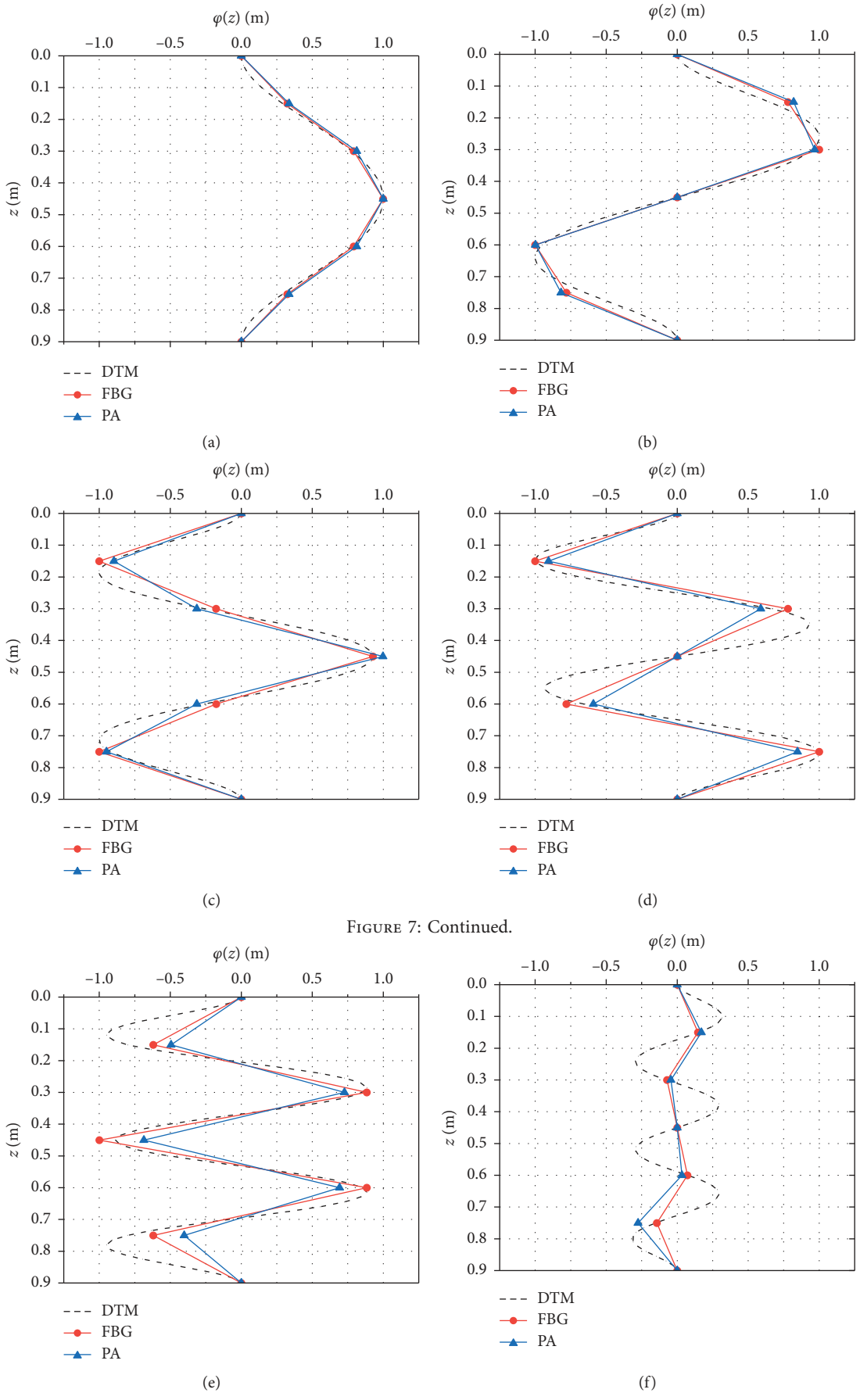

Figure 7: Continued.

Figure 7: Mode shape of the model pipe 1: (a) first mode, (b) second mode, (c) third mode, (d) fourth mode, (e) fifth mode, and (f) sixth mode.

Table 5: Known parameters.

Property	Value
Length of the pipe (l) m	1500
Density of seawater (ρ_w) kg/m^3	1025
Density of drill pipe (ρ_s) kg/m^3	7850
Elastic modulus of steel (E) GPa	206
Outside diameter (D) mm	127
Thickness of pipe (δ) mm	9.19
Add mass coefficient (C_a)	1
Mass of tree and tool (W_B) kg	50000

Table 6: Results of DTM and FEM.

Natural frequency (Hz)	1st	2nd	3rd	4th
DTM	0.01248	0.03769	0.06763	0.09893
FEM	0.01135	0.03414	0.06153	0.09011
Error (%)	9	9.4	9	8.9

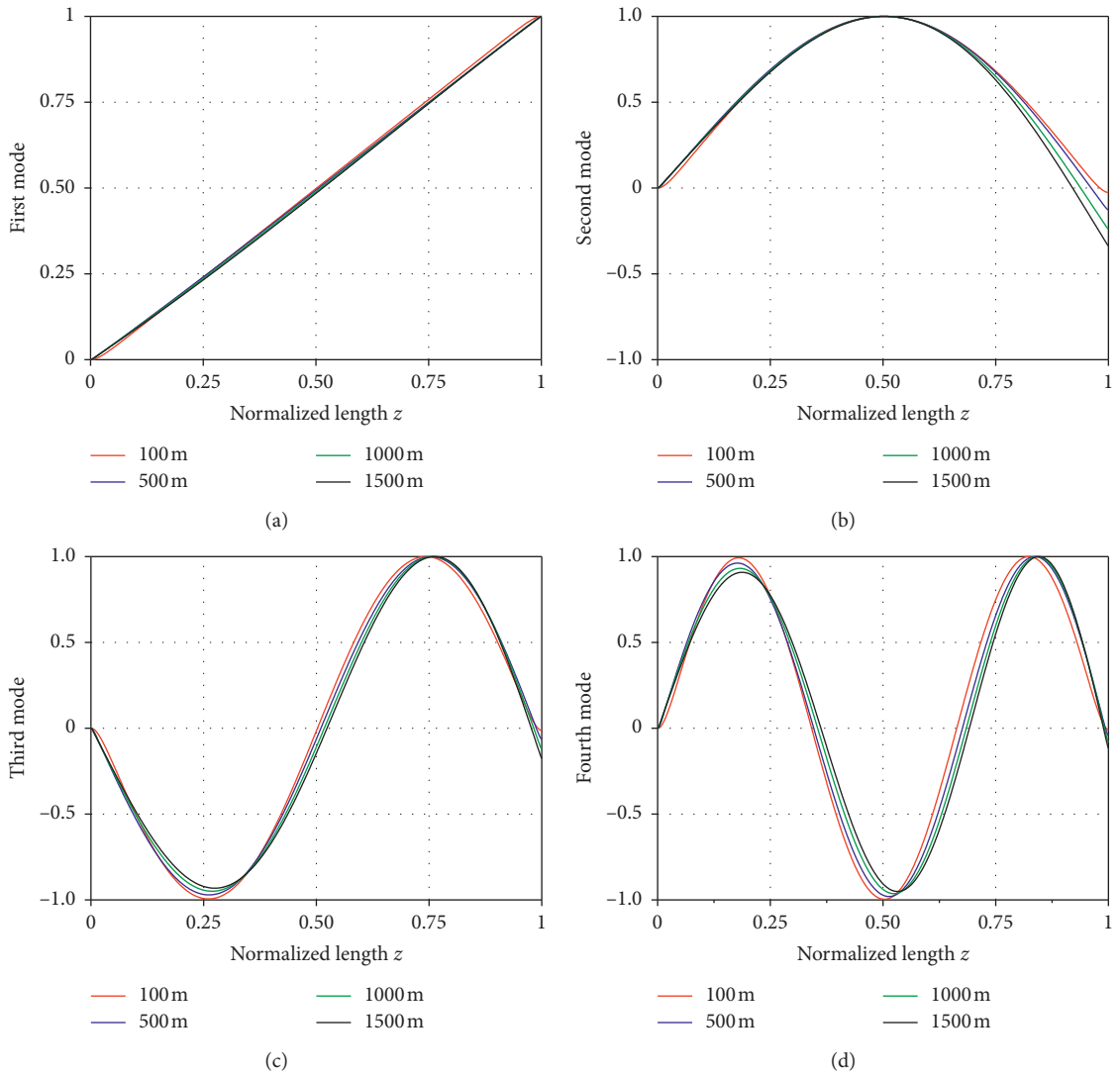

Figure 8: Mode shapes of the pipe of different lengths: (a) first mode, (b) second mode, (c) third mode, and (d) fourth mode.

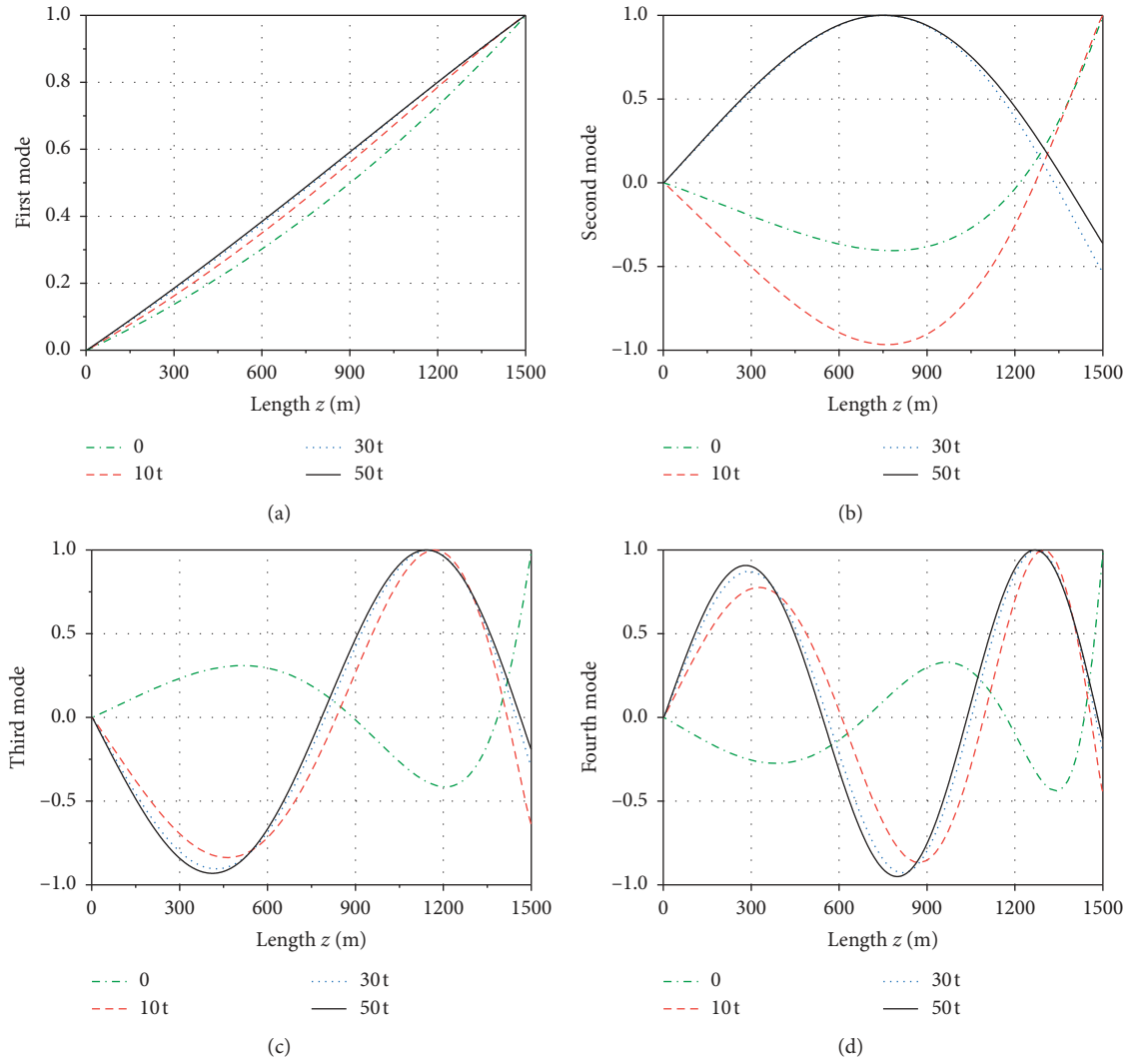

Figure 9: Mode shapes of the pipe with different weight trees: (a) first mode, (b) second mode, (c) third mode, and (d) fourth mode.

sixth-order mode shape are quite different; the measured modal amplitude is significantly smaller than the theoretically calculated amplitude because the test points are too few to show high order modes accurately.

4. Example Calculation and Analysis

4.1. Example. Taking an actual subsea Xmas tree installation process as an example, the known parameters are listed in Table 5:

4.2. Analysis of the Influencing Factors. Table 6 lists natural frequencies that were calculated using DTM and FEM. It can be seen from the table that results of two methods are almost same. Considering that the FEM results can be influenced by the number of finite elements, we believe that the DTM results are closer to the exact solution and more convenient for application.

As noted earlier, the mode shape of the riser can be readily determined using equation (16). Figure 8 shows the first four modes shape of the pipe with different heights. It can be seen from these figures that the mode shape of the pipe remains basically unchanged during the lowering of the tree, but a change in the length affects the mode shape only locally. The amplitude at the end of the pipe increases as the length of the drill pipe increases.

Figure 9 shows the first four mode shapes of the pipe with the Xmas tree having different weights. Under the condition a pipe with a free end, the maximum amplitude is at the end of the pipe, but after hanging the tree, the maximum amplitude does not occur at the end of the pipe. Moreover, as the weight of the tree increases, the vibration amplitude at the end of the drill pipe will decrease.

5. Conclusions

In this paper, the DTM is used to solve the natural frequency and mode shape of a pipe applied in the installation of a subsea Xmas tree, and the results are verified by using PA sensors and FBG sensors. Several conclusions are given as follows:

(1) The frequency obtained using the DTM is acceptable enough for design purposes because the mean error is generally less than 5%, and thus, the frequency of the pipe while lowering a subsea Xmas tree can be determined using the equations and technique proposed in this paper.

(2) According to the experiments in this paper, it can be confirmed that the natural frequency of the vertical cantilever is affected by the length of the beam and the weight of the suspended end when the material properties of the beam are constant. The natural frequency of the beam is inversely proportional to its length and the weight of bottom lumped mass. In other words, during the process of lowering of the tree, the natural frequency of the system will gradually decrease. Meanwhile, the natural frequency of the lowering system can be reduced by adjusting the added weight of the tree to avoid resonance.

(3) The length of the pipe has little influence on the mode shape, but the weight of the tree and the counterweight on the end of the pipe have considerable effects on the mode shape. Relative to a freely suspended drill pipe, the end vibration of a pipe with a lumped mass on one end is more biased towards its equilibrium position.

Nomenclature

D: The outer diameters of the pipe (m)
d: The inner diameters of the pipe (m)
E: The modulus of elasticity (Pa)
I: The area moment of inertia (m^4)
l: The length of the pipe (m)
m_B: The suspend mass at the pipe bottom (kg)
m_e: The effective mass of the pipe per unit length (kg)
m_p: The mass of the pipe (kg)
m_f: The mass of the internal fluid (kg)
m_a: The added mass (kg)
T: The axial tension force of the beam (N)
t: The time (s)
w: The net weight of the pipe per unit length (N)
x: The transverse deflection of the beam axis (m)
z: The coordinate measured along the axis of the pipe (m)
$\overline{z}$: Dimensionless parameter of length
δ: Thickness of pipe
ρ_s: The density of the pipe (kg/m^3)
ρ_w: The density of seawater (kg/m^3)
ρ_f: The density of the internal fluid (kg/m^3)
C_a: The added mass factor
$\varphi(z)$: The product of a spatial function
$\varphi(\overline{z})$: Dimensionless parameter of transverse deflection of the pipe
$\gamma(t)$: A temporal function
ω: The natural frequency of the pipe (Hz)
$\phi(z)$: The differential transformation of the kth-order derivative of a function
$\Phi(k)$: The kth-order differential transformation
λ: The eigenvalue.

Data Availability

The data used to support the findings of this study are available from the corresponding author upon request.

Conflicts of Interest

The authors declare that they have no conflicts of interest with respect to publication of this paper.

Acknowledgments

The authors acknowledge the Ministry of Industry and Information Technology of the PR China for their support through the project "Development of Subsea Vertical Christmas Tree" (Grant no. (2013)420). This work was also funded by National Key Research and Development Project (Grant no. 2016YFC0302900).

References

[1] Y. Bai and Q. Bai, "Chapter 19-subsea manifolds," in *Subsea Engineering Handbook*, Y. Bai and Q. Bai, Eds., Gulf Professional Publishing, Houston, TX, USA, pp. 571–632, 2010.

[2] Y. Wang, H. Tuo, L. W. Li, Y. Zhao, H. Qin, and C. An, "Dynamic simulation of installation of the subsea cluster manifold by drilling pipe in deep water based on orcaflex," *Journal of Petroleum Science and Engineering*, vol. 163, pp. 67–78, 2018.

[3] D. W. Dareing and T. Huang, "Natural frequencies of marine drilling risers," *Journal of Petroleum Technology*, vol. 28, no. 7, pp. 813–818, 1976.

[4] A. Soltanahmadi, "Determination of flexible riser natural frequencies using fourier analysis," *Marine Structures*, vol. 5, no. 2-3, pp. 193–203, 1992.

[5] M. S. Triantafyllou and A. Bliek, "The dynamics of inclined taut and slack marine cables," in *Proceedings of the Offshore Technology Conference*, Houston, TX, USA, May 1983.

[6] C. Sparks, "Transverse modal vibrations of vertical tensioned risers: a simplified analytical approach," *Oil & Gas Science & Technology*, vol. 57, no. 1, pp. 71–86, 2002.

[7] S. Krawczyk, "Influence of joint stiffness on the free vibration of marine riser conveying fluid," *Eighth ISOPE Pacific/Asia Offshore Mechanics Symposium*, vol. 55, 2008.

[8] D. J. Montoya-Hernández, A. O. Vázquez-Hernández, R. Cuamatzi, and M. A. Hernandez, "Natural frequency analysis of a marine riser considering multiphase internal flow behavior," *Ocean Engineering*, vol. 92, pp. 103–113, 2014.

[9] Y. Chen, Y. H. Chai, X. Li, and J. Zhou, "An extraction of the natural frequencies and mode shapes of marine risers by the method of differential transformation," *Computers & Structures*, vol. 87, no. 21-22, pp. 1384–1393, 2009.

[10] W. P. Howson and F. W. Williams, "Natural frequencies of frames with axially loaded timoshenko members," *Journal of Sound and Vibration*, vol. 26, no. 4, pp. 503–515, 1973.

[11] Y. Cheng, J. K. Vandiver, and G. Moe, "The linear vibration analysis of marine risers using the wkb-based dynamic stiffness method," *Journal of Sound and Vibration*, vol. 251, no. 4, pp. 750–760, 2002.

[12] Y. Si, K. Ye, F. W. Williams, and D. Kennedy, "Theory and algorithm of the exact method for free vibration problems of skeletal structures," *Engineering Mechanics*, no. S1, pp. 1–6, 2005.

[13] L.-Y. Xi, X.-F. Li, and G.-J. Tang, "Free vibration of standing and hanging gravity-loaded rayleigh cantilevers," *International Journal of Mechanical Sciences*, vol. 66, pp. 233–238, 2013.

[14] L. N. Virgin, S. T. Santillan, and D. B. Holland, "Effect of gravity on the vibration of vertical cantilevers," *Mechanics Research Communications*, vol. 34, no. 3, pp. 312–317, 2007.

[15] T. Anye and W. Ziguo, "Natural frequencies of transverse vibration of cantilever rayleigh beams," *Journal of Jishou University (Natural Science Edition)*, vol. 38, no. 2, pp. 26–31, 2017.

[16] F. Mirzaee, "Differential transform method for solving linear and nonlinear systems of ordinary differential equations," *Applied Mathematical Sciences*, vol. 5, no. 70, pp. 3465–3472, 2011.

[17] S. Shali, S. R. Nagaraja, and P. Jafarali, "Vibration of non-uniform rod using differential transform method," *IOP Conference Series: Materials Science and Engineering*, vol. 225, Article ID 012027, 2017.

[18] C. Mei, "Application of differential transformation technique to free vibration analysis of a centrifugally stiffened beam," *Computers & Structures*, vol. 86, no. 11-12, pp. 1280–1284, 2008.

[19] S. H. Ho and C. K. Chen, "Analysis of general elastically end restrained non-uniform beams using differential transform," *Applied Mathematical Modelling*, vol. 22, no. 4-5, pp. 219–234, 1998.

[20] H. Qin, J. Liu, W. Xiao, and B. Wang, "Quasistatic nonlinear analysis of a drill pipe in subsea xmas tree installation," *Mathematical Problems in Engineering*, vol. 2019, Article ID 4241363, 9 pages, 2019.

[21] J. F. Doyle, *Wave Propagation in Structures: An FFT-Based Spectral Analysis Methodology*, Springer-Verlag, Berlin, Germany, 1989.

[22] I. H. A.-H. Hassan, "On solving some eigenvalue problems by using a differential transformation," *Applied Mathematics and Computation*, vol. 127, no. 1, pp. 1–22, 2002.